PHYSICAL REVIEW B VOLUME 5, NUMBER 8 15 APRIL 1972

# Interaction between Thermal Phonons and Dislocations in LiF†‡

A. C. Anderson and M. E. Malinowski*
*Department of Physics and Materials Research Laboratory,*
*University of Illinois, Urbana, Illinois* 61801
(Received 12 November 1971)

Thermal conductivity measurements on deformed LiF crystals from 0.04 to 0.8 K have indicated a strong polarization- and frequency-dependent dynamic scattering of thermal phonons by mobile dislocations. Heat-pulse experiments at 3.6 K have verified both the strength and polarization dependence of the scattering mechanism. The scattering of thermal phonons by sessile dislocations was too weak to be detected.

## I. INTRODUCTION

Early estimates[1-3] of the contribution of phonon scattering by sessile dislocations to the thermal resistivity of LiF and similar materials failed to agree with experiment by a factor of $10^2$–$10^3$, although the expected $T^2$ temperature dependence was frequently observed.[4] Later calculations by Ohashi[5] appeared to improve this factor by approximately $10^2$. In addition, it was postulated that cooperative effects involving spatial arrays of dislocations might increase the effective scattering,[4,6,7] although it was found that in certain cases the scattering would actually be reduced.[8,9] In general, it could be argued that theory and experiment were in reasonable accord when one considered such factors as the difficulty in ascertaining accurate dislocation densities in the experimental samples.[10]

On the other hand, it also has been proposed that dynamic scattering of phonons by mobile dislocations might be much more effective than static strain field scattering and hence provide for better agreement with experiment.[11-13] The dynamic interaction of phonons with mobile dislocations has frequently been assumed in connection with internal friction measurements,[1] and direct evidence for such a mechanism has been found in ultrasonic measurements.[14]

It was the purpose of the work reported below to ascertain, for LiF, the relative importance of the two classes of interactions discussed above, namely, static scattering versus dynamic scattering. Thermal-conductivity measurements were used to determine the temperature or frequency dependence of the interaction, and ballistic phonon experiments were used to determine the mode and polarization dependence. $\gamma$ irradiation was utilized to introduce point defects and hence render sessile any mobile dislocations introduced by controlled deformation of the samples.

The experimental techniques are described in Sec. II, the results and discussion, including a comparison with previous work, in Sec. III, a comparison with theory in Sec. IV, and the conclusions in Sec. V. In brief, it was observed in these measurements that a strong dynamic interaction existed for one thermal phonon mode only, the slow transverse mode, and that the interaction of all modes with a static dislocation was very weak.

## II. EXPERIMENTAL TECHNIQUES

### A. Thermal Conductivity

Harshaw optical-grade LiF crystals approximately $0.5\times0.5\times5$ cm in size were used in the thermal-conductivity measurements. The long axis of each crystal was in the [110] direction with the sides oriented in the $[\bar{1}10]$ and [001] directions. Less expensive NaCl crystals were not used, since they recover more rapidly[15] after deformation and also have a tendency to crack on thermal cycling. It is also more difficult to obtain reliable dislocation densities in NaCl using the etch-pit technique. Each sample, prior to measurement, was sandblasted on all surfaces with a home-built unit using airborne 27-$\mu$ aluminum-oxide abrasive driven at a pressure of roughly 4 atm. This treatment reduces the specular reflection of phonons from the crystal surfaces.

Dislocations were introduced into the crystal using a shearing technique suggested by Schwenker and Granato.[14] Before shearing, the crystals were mounted in aluminum holders[16] so that the $(\bar{1}10)$ faces could be polished flat to about $2.5\times10^{-4}$ cm using, in the final step, 1-$\mu$ aluminum-oxide powder and alcohol on a granite block. The crystals were then placed in the shearing jig as indicated in Fig. 1 using Teflon tape between the crystal and the stainless-steel jaws to relieve any uneven stress. Force was applied to the movable jaws or clamps by a Tinius Olsen press.

This method of straining the crystal resulted in a walled area of dislocations approximately 0.1 cm thick containing a rather uniform dislocation density as determined by an etch-pit technique.[17,18] The etch-pit densities were found for both the "wall" and background regions on the (001) faces by photographing through a Zeiss metallurgical microscope.

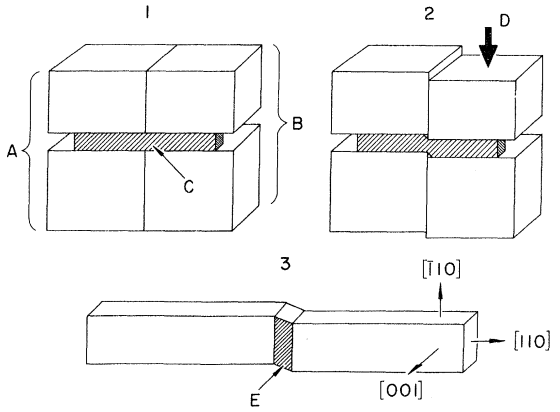


FIG. 1. Apparatus used to deform the LiF samples. A and B represent fixed and movable stainless-steel clamps, respectively, and C is the crystal. Force is applied to the movable clamp at D, resulting in a 1-mm-wide region of dislocations at E in an enlarged view of the crystal. The offset at E has been exaggerated. The actual offset ranged from 0.002 to 0.01 cm.

Assuming that each pit corresponded to a single dislocation, the background was found to contain a density of $(3-4)\times10^6$ cm$^{-2}$, while the wall region contained $(3-5)\times10^7$ cm$^{-2}$. One of the crystals was also cleaved several times on (100) planes and etched. The count in the wall region was $5\times10^6$ cm$^{-2}$, similar to the background region. Hence the dislocations would appear to be predominately edge-like in character, since the etch-pit count in the wall region on the (001) faces was an order of magnitude larger than for the (100) faces.

A $^{60}$Co source of $\gamma$ rays was used to introduce pinning points. The dose in roentgen units (R) was measured using a Victoreen radiation dosimeter. All irradiations were performed at room temperature at a typical rate of 0.5 R/sec.

The experimental arrangement is shown in Fig. 2. The three resistance thermometers[19] permitted the thermal conductance to be measured over a region containing the wall of dislocations ($r$–$n$) and also over a region containing no additional dislocations ($n$–$f$). Thermometers $n$ and $f$ were calibrated to an accuracy of $\lesssim 2\%$ over the temperature range of the measurements by comparison to a magnetic thermometer[20] which had been calibrated against the vapor pressure of liquid $^3$He. Thermometer $r$ was not calibrated and served to keep the point $r$ on the sample at a constant temperature during a measurement via electronic regulation of the dilution refrigerator. To check on any error caused by a residual heat leak, the positions of the thermometers were interchanged and the resistors recalibrated against the magnetic thermometer. No change in calibration could be observed and hence there was no significant heat leak along the sample. The uncertainty in the calculated thermal conductivity $\kappa$ was $\lesssim 4\%$, which included the uncertainties in temperature calibration, sample dimensions, and heater power.

### B. Heat Pulses

Heat-pulse measurements allow a determination of the phonon mode being observed by measuring the time of flight of a pulse between generator (an electrical heater) and detector or bolometer (a current biased superconducting film).[21]

The optical-grade LiF crystals were oriented identically to those used in the thermal-conductivity measurements, and dislocations were also inserted in the same manner. The crystals were about 1 cm on a side and 0.6 cm thick. The sides were sand-blasted; the ends were polished using 1-$\mu$ aluminum-oxide abrasive in alcohol on a granite block in the final step. The crystals were degreased and silver contacts were painted on. Then the thin-film detectors and heaters were evaporated on at a residual pressure of about $10^{-6}$ Torr while monitoring their resistances. The manganin heaters had a room-temperature resistance of $\approx 50\ \Omega$; the (96-at.% In–4-at.% Sn) detectors had a room-temperature resistance of 10–100 $\Omega$. (Attempts to use aluminum detectors yielded poor results.) Electrical leads were attached using silver paint as a glue. The

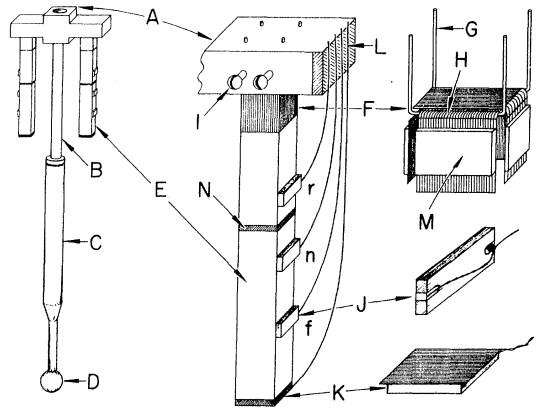


FIG. 2. Thermal-conductivity apparatus: A is the copper block which screwed onto a dilution refrigerator; B, C are thermally conducting support for the cerous magnesium nitrate magnetic thermometer at D; E is the LiF single-crystal sample; F is the coilfoil thermal ground for sample, to prevent cracking of sample with thermal cycling; G are copper support wires; H are indium solder thermal joints; I are copper bolts; J are carbon resistance thermometers; K is the electrical heater; L are electrical leads thermally grounded through cigarette paper and Ge 7031 varnish; M are fiber blocks to press Apiezon N-grease coated foils against sample when wrapped with thread; N is the region of high dislocation density. A thermal shield at 0.7 K completely surrounded the apparatus.

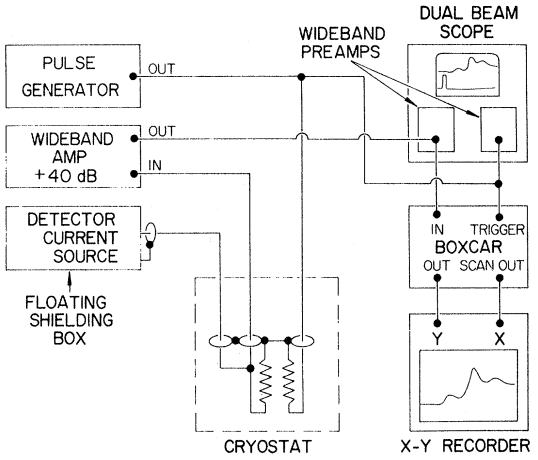


FIG. 3. Electronics for heat-pulse measurements. The electrical grounds were selected by trial and error to give the greatest attenuation to spurious coupling between input and output.

films and paint withstood thermal cycling, provided moisture was not allowed to condense onto the apparatus. The detectors had a sensitivity of about 1 V/K.

The samples were immersed in liquid $^4$He at a controlled temperature of 3.6 K. The electronics are shown schematically in Fig. 3. The applied pulses were $10^{-7}$ sec or less in duration and could be varied from 0.5 to 20 V in amplitude. Generally the temperature of the resulting thermal pulses was kept within 0.2–0.5 K of the ambient.

The signal obtained from the detector depended on the relative positions and sizes of the heater and detector because of phonon focusing.[22,23] The effects of focusing and the size and placement of heater and detectors are depicted in Fig. 4. The large detector C was required in order to detect all three modes simultaneously. However, to be certain that the signals were being properly identified, samples were also run with a small detector at positions B or A. Position A, in the [110] direction, displayed the fast transverse and longitudinal modes, while position B displayed the slow transverse as well as longitudinal mode. Each measured velocity agreed with theoretical predictions as well as with previous experiments. Since detector B was closer to the side of the sample, the "background" due to diffuse scattering of phonons from the walls was larger than for detector A. For the same reason the background for the large detector C was quite large as will be shown below.

## III. RESULTS AND A COMPARISON WITH PREVIOUS WORK

Most of the thermal-conductivity measurements were performed on two LiF crystals which were designated samples 2 and 4. The dimensions of crystal 4 in the [001] and [$\bar{1}$10] directions were 7% larger than for crystal 2. The conductivities of each crystal in the two regions $r$–$n$ and $n$–$f$ (Fig. 2) were measured before and after the wall of dislocations was introduced. Then several runs were made after the crystals were $\gamma$ irradiated differing amounts. With enough irradiation the dislocations were expected to be rendered effectively immobile by the point defects produced by $\gamma$ rays. If this condition prevailed there would be no dynamic scattering, but only static scattering by the dislocation strain field and core.

A preview of the data is shown in Fig. 5 for crystal 2. Here the thermal conductivity $\kappa_w$ of the section between thermometers $r$ and $n$ containing the wall region has been plotted for several runs, including that prior to shearing, after shearing, after a brief exposure to $\gamma$ rays, and after a long exposure to $\gamma$ rays. Both the shearing and the exposure to $\gamma$ irradiation did indeed produce changes in $\kappa_w$, but not nearly as large a change as would have been expected from a review of the existing literature. Nevertheless it may be noted qualitatively that shearing decreased the thermal conductivity by about 50% over the temperature range investigated and that a long exposure to irradiation returned the conductivity to the magnitude measured prior to the insertion of dislocations, the dislocations of course still being present. Hence the scattering of phonons by fully pinned, static dislocations is weak, whereas the scattering by unpinned or mobile dislocations is strong and is caused by a dynamic mechanism. We now retreat and take a more systematic look at the data.

The conductivities $\kappa_B$ of the two crystals were measured before they were strained or deformed. One would then expect a $T^3$ temperature dependence

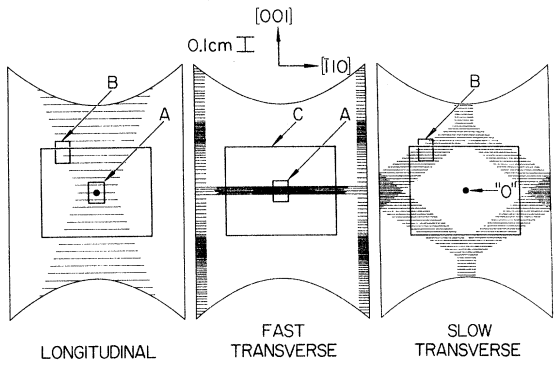


FIG. 4. Focusing of phonons in the [110] direction in LiF. These somewhat simplified diagrams display qualitatively the relative intensities of the three phonon modes on the front surface of a crystal 0.6 cm thick with a point source of heat located on the rear surface at 0. The positions and sizes of detectors A, B, and C are shown.

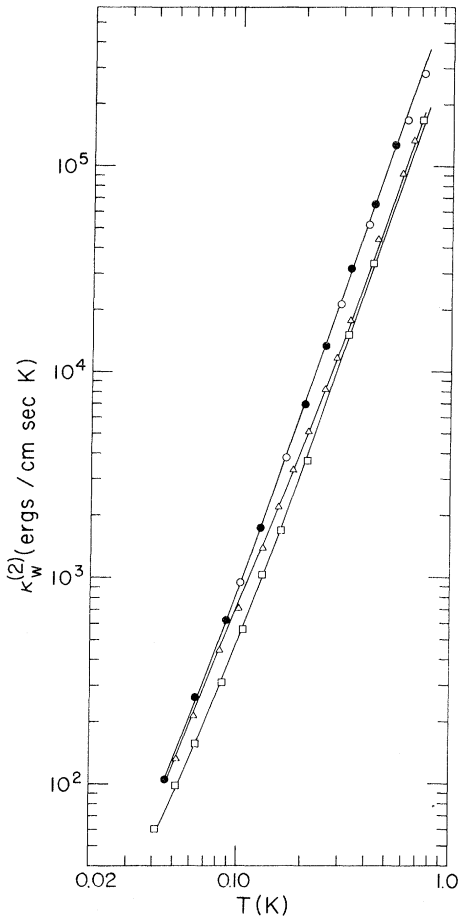


FIG. 5. Thermal conductivity of sample 2 for the region containing the wall of dislocations, $\kappa_\omega^{(2)}$ vs temperature (some data have been omitted for clarity); ●—undeformed crystal; □—deformed crystal; △—1000-R total irradiation; ○—136 000-R total irradiation.

resulting from a constant mean free path due to boundary scattering. The results are plotted in Fig. 6 in the form $\kappa_B T^{-3}$ in order to remove most of the temperature dependence and allow the full resolution of the apparatus to be exploited. The conductivity does vary precisely as $T^3$ except below $\approx 0.1$ K. We believe the increase in $\kappa_B T^{-3}$ below 0.1 K to be caused by the onset of partial specular reflection from the lightly sandblasted walls. Harrison,[24] having used a similar abrading technique but a higher driving pressure, reported a $T^3$ dependence to somewhat lower temperatures for LiF. A similar deviation, but beginning near 2 K, has been reported for the harder crystal sapphire which was also roughened on the surfaces.[25]

The theoretical values for $\kappa_B$, assuming boundary scattering and taking into account focusing[26] and end effects,[27] are shown by the arrows in Fig. 6 for each sample. The experimental data in the $T^3$ region lie $\approx 15\%$ too low, although the calculated or theoretical ratio $\kappa_B{}^{(4)}/\kappa_B{}^{(2)} = 1.07$ which is in good agreement with the ratio of the sample dimensions. (The superscripts refer to samples 4 and 2, respectively.) The theoretical magnitude of $\kappa_B$ is rather sensitive to the mathematical integrating scheme used[3] and hence is somewhat uncertain. The ratio, however, is independent of this problem. Hence the phonon mean free path related to the data of Fig. 6 is most likely limited by boundary scattering. For latter use, the smooth curves drawn through the data of Fig. 6 will be referred to as $\langle \kappa_B \rangle$.

The background thermal conductivities $\kappa_b$, that is, the conductivity measured between thermometers $n$ and $f$ of Fig. 2, are plotted in Figs. 7 and 8. The reduced form $\kappa_b \langle \kappa_B \rangle^{-1}$ is used to remove most of the temperature dependence and to emphasize any changes that might have occurred after the sample was placed in the shearing jig or irradiated. The average of all the data for each sample, represented by the horizontal lines in Figs. 7 and 8, yields $\kappa_b{}^{(2)} \langle \kappa_B{}^{(2)} \rangle^{-1} = 0.93$ and $\kappa_b{}^{(4)} \times \langle \kappa_B{}^{(4)} \rangle^{-1} = 0.89$. Hence neither the shearing operation nor subsequent irradiation caused any significant change in $\kappa_b$, and any changes in $\kappa_w$ are to be associated with dislocations introduced into the wall region by crystal deformation. Small quantitative changes in $\kappa_b$ can be detected in Figs. 7 and 8, but these will be commented upon later.

The fact that phonon scattering by point defects introduced by irradiation cannot be detected in the thermal-conductivity measurements is not surprising. A dose of over $10^8$ R is required to reduce the conductivity by an order of magnitude near 4 K,[28] and the expected temperature dependence of the scattering cross section should vary as $T^4$. The maximum dose used in the present conductivity measurements was $\approx 10^5$ R, and the highest temperature was $\approx 1$ K. Phonon scattering by the $F$

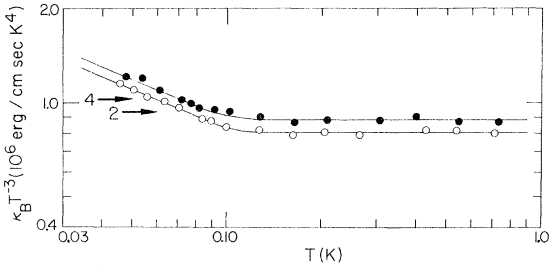


FIG. 6. Reduced boundary-limited thermal conductivity $\kappa_B T^{-3}$ for sample 2 (○) and 4 (●) vs temperature. The values calculated theoretically are indicated by the arrows. Sample 2 had room-temperature dimensions of $0.566 \times 0.587 \times 5.11$ cm, sample 4 had dimensions of $0.599 \times 0.630 \times 5.12$ cm.

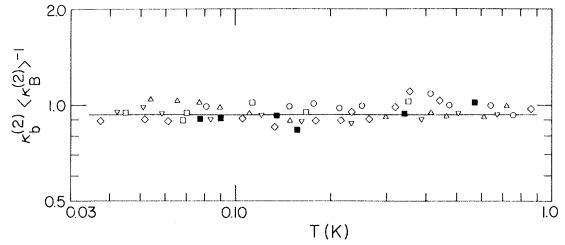


FIG. 7. Reduced background thermal conductivity for sample 2, $\kappa_b^{(2)}\langle\kappa_b^{(2)}\rangle^{-1}$, vs temperature: □ —deformed sample; ■—deformed sample, remeasured; ▽—800-R total irradiation; △—1000-R total irradiation; ◇—26 000-R total irradiation; ○—136 000-R total irradiation.

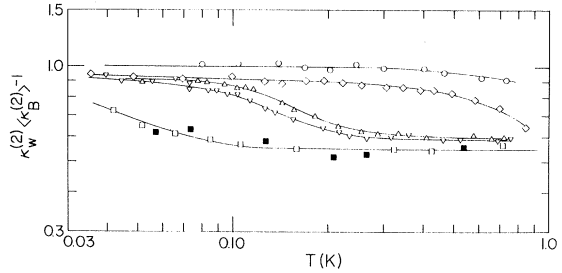


FIG. 9. Reduced thermal conductivity for the wall region of sample 2, $\kappa_w^{(2)}\langle\kappa_B^{(2)}\rangle^{-1}$, vs temperature: □—deformed sample; ■—deformed sample, remeasured; ▽—800-R total irradiation; △—1000-R total irradiation; ◇—26 000-R total irradiation; ○—136 000-R total irradiation.

centers could be detected at 3.6 K after an irradiation of $10^6$ R in the ballistic phonon pulse measurements discussed below.

The effect of dislocations introduced by crystal deformation is shown in Figs. 9 and 10 where again the data are plotted in a reduced form $\kappa_w\langle\kappa_B\rangle^{-1}$. It may be noted that there is a transition or, to avoid confusion, a crossover temperature between $\kappa_w\langle\kappa_B\rangle^{-1}=1.0$, corresponding to boundary limited conductivity, and $\kappa_w\langle\kappa_B\rangle^{-1}\approx 0.5$, corresponding to dislocation limited conductivity. Furthermore, this crossover temperature moves to higher temperature as the irradiation dose is increased. The crossover temperature is plotted against accumulated dose in Fig. 11, where a saturation effect may be noted at high irradiation dosage.

The details of Figs. 9 and 10 will be discussed in Sec. IV. However, one major and surprising feature of these data is that the conductivity is reduced by only ≈50% in contrast to much larger reductions reported previously.[6] The present data are suggestive that only one of the phonon modes was being scattered. In view of the Peach-Koehler relation,[29] the slow transverse mode is most likely to be scattered by edge dislocations in these samples. Assuming the mean free path of the slow transverse phonons to be much less than the sample width and the mean free path of the other two modes to be limited by boundary scattering, the thermal conductivity should be reduced about 50% and exhibit a temperature dependence of $T^3$. This is in rather good agreement with the data of Figs. 9 and 10 where the reduction is (45–47)% and the temperature dependence above the crossover temperature is close to $T^3$.

As a test of this model of polarization-dependent scattering two additional measurements were made, one using thermal conductivity and the other using thermal phonon pulses. The sample used in the thermal-conductivity measurements is shown in Fig. 12. A 1.2-cm length of the crystal was filled with dislocations by repetition of the polishing and shearing technique outlined in Sec. II. The ratio of thermal conductivities $\kappa_N/\kappa_F$ (see Fig. 12) should have been ≈7 if each dislocation exposed the same scattering cross section to each phonon regardless of polarization. The results are also shown in Fig. 12. Rather than a factor of 7, there is only a 5% decrease in $\kappa$. In other

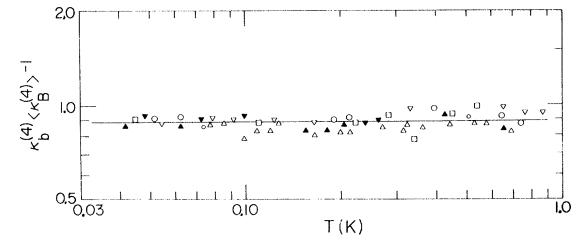


FIG. 8. Reduced background thermal conductivity for sample 4, $\kappa_b^{(4)}\langle\kappa_B^{(4)}\rangle^{-1}$ vs temperature: □—deformed sample; ▽—400-R total irradiation; ▼—400 R, sample remeasured; △—800-R total irradiation; ▲—800 R, sample remeasured; ○—39 500-R total irradiation.

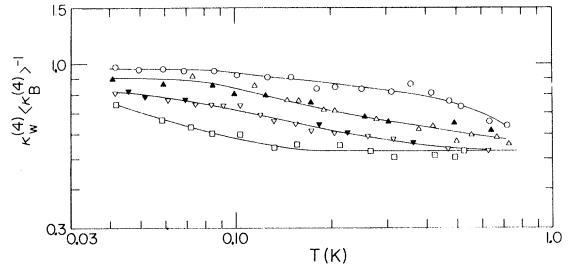


FIG. 10. Reduced thermal conductivity for the wall region of sample 4, $\kappa_w^{(4)}\langle\kappa_B^{(4)}\rangle^{-1}$ vs temperature: □—deformed sample; ▽—400-R total irradiation; ▼—400 R, sample remeasured; △—800-R total irradiation; ▲—800 R, sample remeasured; ○—39 500-R total irradiation.

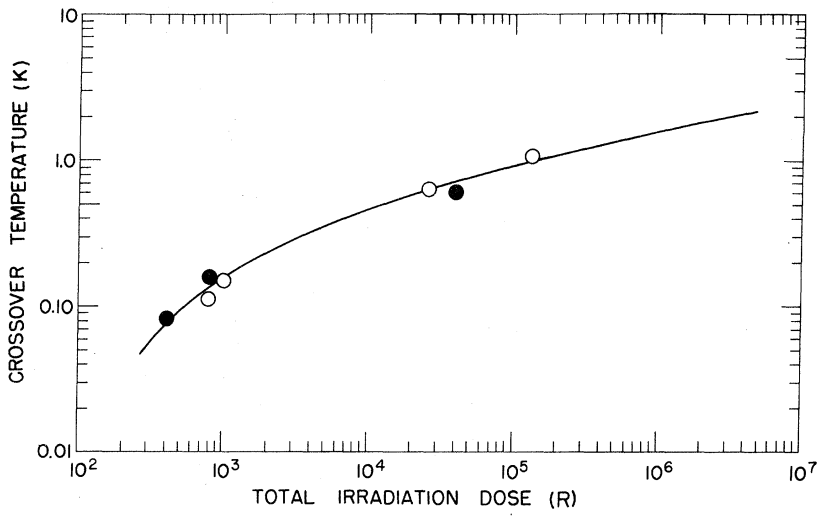


FIG. 11. Crossover temperatures of Figs. 9 and 10 vs total irradiation dose: ○—sample 2; ●—sample 4.

words, the thermal conductivity is essentially *independent* of the number of mobile dislocations present in these measurements. This is consistent with the model suggested above, since reducing the mean free path of the slow transverse phonons even to zero would not further reduce the thermal transport provided almost entirely by longitudinal and fast transverse phonons.

As a further check on the model, the propagation of ballistic heat pulses was observed at 3.6 K using the technique described in Sec. II. By this means it was possible to identify the three individual phonon modes by their time of flight. The results are shown in Fig. 13 before shearing (A), after shearing and the introduction of dislocations (B), and following $\gamma$ irradiation of $10^6$ R (C). The dislocations decreased the relative amplitude of the slow shear mode by ≈80% and the longitudinal mode by ≈25%. The small interaction with the longitudinal phonons probably occurred because some of these phonons were propagating slightly off the [110] direction (see Fig. 4) in which case there results a shear stress in the dislocation slip plane.

Irradiation of $10^6$ R did not fully restore the slow transverse pulse, but from Fig. 11 it would appear that $\gtrsim 10^7$ R would be required to effectively pin the dislocations at 3.6 K. Aside from the problem of time limitations at the Co source, such a large dose would introduce a high concentration of point defects which cause diffuse scattering out of the ballistic pulses. The onset of this effect may be noted in Fig. 13(C), where it is evident that the diffusively scattered phonon background has been increased ≈20% by an irradiation of $10^6$ R.

It therefore has been determined that for the array of dislocations introduced in the present LiF crystals and for the temperature range 0.03–3 K, slow transverse phonons are strongly scattered by mobile dislocations while the scattering of any mode by sessile dislocations cannot be detected.

With these results in mind, we may return to a discussion of Figs. 7 and 8 of the "background"

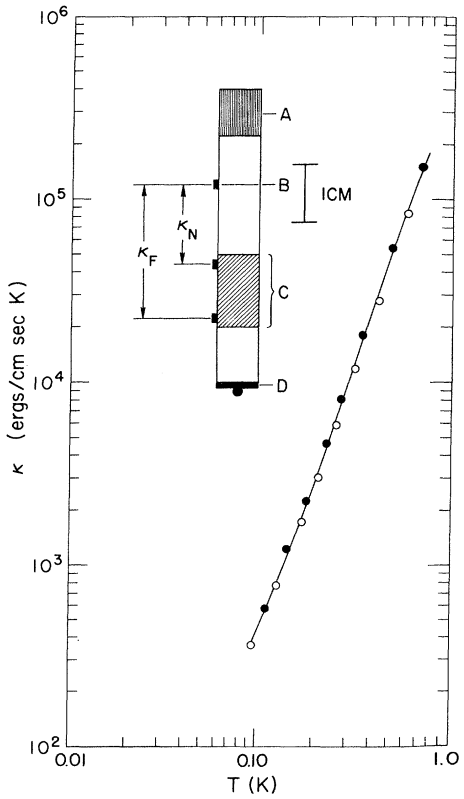


FIG. 12. Insert shows the arrangement for measuring the thermal conductivities of a sample containing an extended region of high dislocation density, C. A—coilfoil thermal ground; B—regulating thermometer; D—electrical heater. The two conductivities measured are plotted vs temperature: ●—$\kappa_N$; ○—$\kappa_F$.

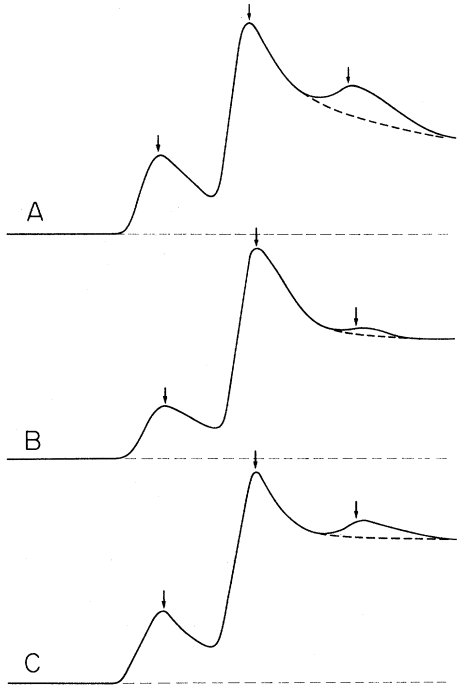


FIG. 13. The effect of dislocation scattering on heat pulse amplitude for a LiF sample 0.6 cm thick. The curves, with time increasing to the right, were obtained from the box car integrator of Fig. 3. A—undeformed sample. The calculated arrival times of the longitudinal, fast transverse, and slow transverse ballistic phonons are indicated, respectively, by the three arrows. The amplitude of the slow transverse pulse is measured relative to the background of diffusively scattered phonons represented approximately by the heavy broken line. Most of this background resulted from scattering by the walls of the crystal and would not have been present if a sample of larger cross section had been available. B—deformed sample. A large reduction in the slow transverse pulse and a small reduction in the longitudinal pulse may be noted. The resultant increase in the diffusive background near the end of the trace may also be observed. C—deformed sample after $10^6$ R of irradiation. The slow transverse pulse had not fully recovered its original amplitude at this dose. The increase in the diffusive background due to scattering of the previously ballistic phonons from the $\gamma$-ray-induced color centers may be readily noted.

thermal conductivity $\kappa_b$. The density of grown-in dislocations in this region of the crystal was $\approx 10^6$ cm$^{-2}$. Had these dislocations been mobile the dynamic scattering of phonons should have been readily detected if the scattering cross section were as large as for the dislocations intentionally introduced. Thus it appears that the grown-in dislocations in the present samples were already completely pinned. Evidence for strong pinning of grown-in dislocations has been reported elsewhere.[17] On the other hand, Thacher[30] reported phonon scattering from grown-in dislocations at a density of $\approx 10^7$ cm$^{-2}$. It may be, therefore, that the mobility of grown-in dislocations depends on the density of dislocations (and perhaps impurities) and on the thermal history of the specimen.

The data of Thacher[30] can be qualitatively explained if it is assumed that some polarization-dependent scattering was also present in his samples containing $\approx 10^7$ cm$^{-2}$ dislocations. In brief, he found that the proportionality constant $\alpha$ in $\kappa = \alpha T^3$, which should be and indeed was related to boundary scattering, was strongly influenced by dislocations in the crystal interior. This is precisely what has been found in the present work and undoubtedly the explanation is the same. Some phonon mode had been "depopulated" of thermal carriers relative to other modes by action of the dislocations.

The thermal-conductivity experiment on LiF which most closely resembles the present work was that of Taylor *et al.*[7] There a long LiF crystal was bent such that the bent region was $\approx 1$ cm in length and contained a dislocation density of $\approx 2\times10^7$ cm$^{-2}$. The grown-in dislocation density was $\approx 5\times10^5$ cm$^{-2}$. The conductivity in the deformed region was roughly 50% that of the undeformed crystal. Again we suggest that the explanation is not cooperative scattering due to a special spatial array of dislocations as discussed by Taylor *et al.*, but rather the polarization-dependent depopulation of one mode of the thermal carriers as observed in the present work.

Some data are available on LiF crystals deformed by compression.[6,31] The dislocation densities had a range of $(2\text{–}40)\times10^7$ cm$^{-2}$. In these samples the thermal conductivity was reduced by more than an order of magnitude by deformation, and the effect did not saturate with increasing numbers of dislocations. This may be compared to a saturation at a factor of $\approx 2$ in the present measurements (see Figs. 9, 10, and 12). Three comments can be made concerning these results. First, at high dislocation densities and at higher temperatures (2–30 K for Refs. 6 and 13) the $\kappa \propto T^2$ temperature dependence due to scattering by static dislocations could become important, although presumably dislocations introduced by compression would also be mobile. Second, any relaxation that occurs *between* the three phonon modes would cause greatly reduced thermal transport. We have in mind here processes which exchange energy between phonon modes, that is, that produce local thermal equilibrium between a mode having a very short mean free path and those of long mean free path. This might occur at abraded surfaces.[32] Hence even the geometry of the experimental measurement could influence the measured conductivity, and the results would be essentially impossible to analyze. Finally, the thermal con-

duction in the crystals deformed by compression was measured in the [100] direction. In this case, all three phonon modes would be scattered if screw dislocations were also present. This would in itself explain the large reduction in $\kappa$ and the proportionality between $\kappa$ and the dislocation density observed in crystals deformed by compression.

The influence of rethermalization between modes mentioned above may be seen qualitatively in Figs. 7 and 9. The ratio of $\kappa_b\langle\kappa_B\rangle^{-1}$ is less than unity because of the proximity of the dislocation wall, a sort of "end effect." With increasing irradiation the ratio moves towards unity. Also the crystal of narrower cross section should thermalize more quickly since the phonons then scatter spectrally (in energy and polarization) more frequently. Indeed, the narrower crystal (2) does have a ratio $\kappa_b\langle\kappa_B\rangle^{-1}$ closer to unity. In effect, the wall of dislocations is the acoustic analog of the Polaroid sheet in the field of optics.

## IV. COMPARISON WITH THEORY

The maximum of the integrand in the Debye integral for the specific heat occurs at $h\nu = 3.8kT$. Since the same function appears in the thermal conductivity integral, we for convenience define the dominate phonons at temperature $T$ to have a frequency $\nu_D = 3.8\ kT/h \simeq 10^{11}\ T$ (Hz/K). Using this value, the scattering rates ($\tau^{-1}$) calculated for several processes are plotted in Fig. 14. The horizontal line C is the frequency-independent boundary or surface-scattering rate appropriate to a sample of roughly 0.6-cm mean width, that is, appropriate to crystals used in the present measurements. As mentioned in Sec. III, the data are in agreement with this scattering rate for LiF crystals containing fully pinned dislocations.

Curves D, E, and F of Fig. 14 give $\tau^{-1}$ for the scattering of phonons in LiF by the strain fields of static dislocations as calculated by Ohashi,[5] Carruthers,[3] and Klemens,[2] respectively. A dislocation density of $4\times10^7$ cm$^{-2}$ has been assumed, similar to the etch-pit density for our samples. By simply comparing Fig. 7 (open circles) with Fig. 14 (line D) near 1 K, it may be concluded that Ohashi's results are too large by roughly an order of magnitude for pinned and hence static dislocations. By considering the data of Figs. 7 and 12, it is concluded that $\tau^{-1}$ due to static dislocation scattering is about 50 times less than for boundary scattering near 1 K. Hence our results are in complete disagreement with Ohashi's calculation, but are consistent with the earlier calculations of Klemens and Carruthers. However, since we never detected scattering due to sessile dislocations, even the scattering rates calculated by the later two authors could conceivably be too large.

We next confront the problem of the dynamic scattering of phonons by mobile dislocations, but here both the data and the theories are more obscure than for static scattering. The data are obscure since the details of the temperature or frequency dependence are almost completely masked by the thermal transport provided by longitudinal and fast transverse phonons (Figs. 9 and 10). The theoretical picture is confused by a variety of models and by a lack of explicit predictions which may be applied to the data. The one detail concerning dynamic phonon scattering by mobile dislocations where theory and experiment agree is the polarization dependence. The data of Fig. 13 are in agreement with the Peach-Koehler formula.[29]

Several dynamical models of dislocation behavior have been developed.[1] The most simple approach is the "string" model where the dislocations are considered to be elastic strings firmly fixed only at the pinning points. Various kink models proceed one step further and attempt to take into consideration the atomic nature of the lattice and hence the Peierls potential. In brief, the dislocation can be visualized as a string of beads lying on a corrugated sheet which represents the undulating Peierls valleys.[33] Both models have been useful in explaining

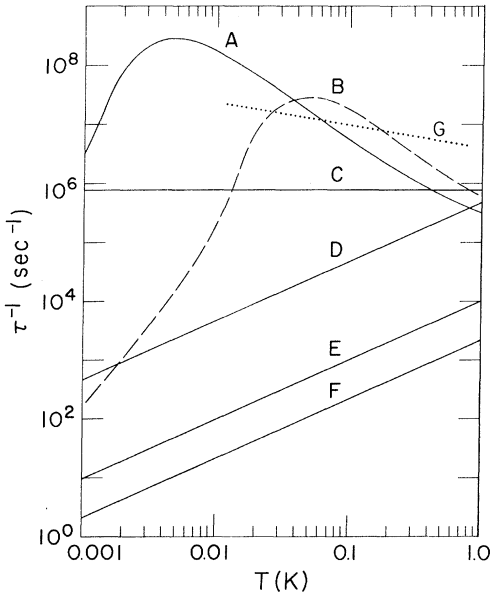


FIG. 14. Theoretical scattering rates $\tau^{-1}$ for a LiF sample having a mean width of 0.6 cm and a dislocation density of $4\times10^7$ cm$^{-2}$, for dominate phonons at temperature $T$: A—resonant scattering assuming an average dislocation loop length of $10^{-4}$ cm (Ref. 35); B—resonant scattering assuming an average dislocation loop length of $10^{-5}$ cm (Ref. 35); C—boundary scattering; D—strain field scattering according to Ohashi (Ref. 5); E—strain field scattering according to Carruthers (Ref. 3); F—strain field scattering according to Klemens (Ref. 2); G—dynamic scattering according to Ninomiya (Ref. 13).

a variety of phenomena.

A third approach[1] is to find the excitations of the crystal as a whole, but including any influence due to the presence of the dislocations. The result is a set of local modes with which the phonons may interact, be absorbed and reemitted. The effect is somewhat analogous to the passage of photons through a gas having excited states within the photon spectrum.[34]

Although the third approach is the most appropriate to a thermal transport measurement, we look first at the more simple string model. The scattering rate predicted by the string model[35] is shown in Fig. 14 for an exponential distribution of loop lengths.[36] Curve A is for an average loop length or distance between pinning points of about $10^{-4}$ cm; curve B is for an average loop length of about $10^{-5}$ cm. The boson spectrum of the phonons has not explicitly been folded into these curves. However, this would not significantly change the shape of curves A or B since the half-width of the phonon spectrum is much narrower than the half-width of curves A or B. A less-realistic $\delta$-function distribution of dislocation loop lengths would move the peaks in A and B about a factor of 3–4 higher in temperature and decrease their half-widths.

In terms of the string model, the crossover temperatures of Figs. 9 and 10 would be represented roughly by the intersection of a curve such as A or B in Fig. 14 with line C. For each of the strained but unirradiated crystals this occurs at 0.04 K which would correspond to an average loop length $L_0 \simeq 3\times10^{-6}$ cm. This is over an order of magnitude shorter than is usually quoted from ultrasonic measurements.[37–39] A simple explanation of this apparent discrepancy would be a set of weak pinning points which would be effective at the small vibrational amplitude of the dislocations in the present experiments. This amplitude is, after all; the smallest physically possible, since the dislocations are in thermal equilibrium at the temperature of the measurement. On the other hand, a macroscopic vibrational magnitude associated with ultrasonic measurements would allow the dislocation to be held fixed only at a set of stronger pinning points. It would therefore follow that the ultrasonic parameters would be amplitude dependent to the lowest amplitudes. The weak pinning points could easily be supplied by impurities in the present samples.

But there are other problems with the string model. If $L_0 \simeq 3\times10^{-6}$ cm as required by the data of Figs. 9 and 10, then the phonon mean free path should again be 0.6 cm or longer above $\approx$2 K for a freshly deformed crystal. From Fig. 13(B) the note that this is not so. One could argue that the reradiation damping calculated by Eshelby[40] and used in the string model was too small, that the curves A or B of Fig. 14 should be moved higher on the graph. For example, $L_0 \simeq 2\times10^{-6}$ cm and an attenuation about a factor of 50 larger than the Eshelby value would be consistent with the present data for freshly strained crystals.

It is not necessary to introduce this factor of 50, however, if we include the scattering mechanism investigated by Ninomiya.[13] Whereas the Garber-Granato calculation[35] considers the interaction of phonons with standing wave modes (fundamental and overtones) on the elastic string, Ninomiya considers essentially the interaction of phonons with traveling waves on an elastic string of infinite extent. The interaction is largest when the projection of the phonon wave vector parallel to the string is equal to the wave vector of the traveling wave on the string. Hence the interaction is independent of frequency, but has a "resonance" relative to the angle the phonon approaches the string. This is analogous to the excitation of Rayleigh waves on the surface of a solid resulting from the incidence of dilitational bulk waves. The resulting scattering rate calculated by Ninomiya for LiF is represented roughly by line G in Fig. 14. (The assumptions used in this calculation were not presented explicitly.) Since the dislocation lines are not infinite, i.e., there are pinning points, line G should have a low-frequency cutoff corresponding, for strong phonon interaction and hence short radiative lifetimes, to $L_0$ roughly equal to $\frac{1}{2}$ wavelength of the dislocation traveling wave. This coincides with the resonance condition for the standing waves. A complete calculation would therefore appear to produce a smooth merging between curves such as A or B in Fig. 4 and line G. The combined result would adequately account for all the present data, although the data of Ref. 7, which extend to higher temperatures, would require a larger scattering cross section than provided by Ninomiya's result.

With irradiation and the shortening of the dislocation loop lengths, the crossover temperature of Figs. 9 and 10 moves up to at least 1 K corresponding, in terms of the string model, to $L_0 \approx 5\times10^{-8}$ cm. This is of the order of the lattice spacing, and the model itself is not applicable in this limit.

A consideration of the kink model[41] adds little to the above discussion. For a very high density of kinks, the curves A and B of Fig. 14 again apply, whereas for a lower density of kinks the peak in $\tau^{-1}$ moves to lower temperatures (frequencies) and decreases in magnitude. Hence the kink model has even less of a tendency to agree with the present experimental data than the simple string model.

In this kink model the dislocation is assumed to lie in the Peierls potential troughs with only the kinks free to move in a direction parallel to the troughs. One could alternatively picture the kinks

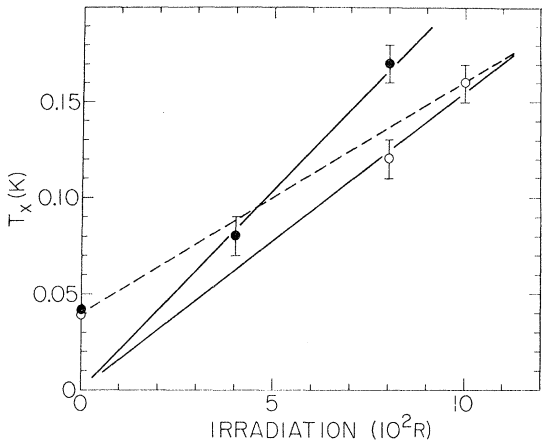


FIG. 15. Plot of $T_x$ vs $\gamma$-irradiation dose for sample 2 (O) and 4 (●). The error bars reflect the uncertainty in obtaining a consistent crossover temperature $T_c$ from Figs. 9 and 10. Since $T_x = T_c[1 - (\sigma_P/4\pi^2\rho\delta^2 T_c^2 b^2 \times 10^{22})]^{1/2}$, the broken line corresponds to a zero Peierls stress $\sigma_P$, i.e., $T_x = T_c$, while the solid lines correspond to a finite Peierls potential.

also lying in a weaker Peierls potential, hence remaining fixed in position, and the dislocations moving *within* their respective Peierls potential and in a direction perpendicular to the troughs. The resonant angular frequency $\omega_0$ for lines of average length $L$ then becomes roughly

$$\omega_0 = [(\sigma_P/\rho b^2) + (\pi^2 G/2L^2\rho)]^{1/2}, \quad (1)$$

where $\sigma_P$ is the Peierls stress, $\rho$ is the crystal mass density, $b$ is the magnitude of the Burger's vector, and $G$ is the elastic modulus. The frequency $\omega_0$ may vary by a factor of about two depending on what approximation is adopted for the dislocation mass, etc., but this would not significantly alter the results to be obtained.

With irradiation the average loop length $L$ should vary with dose $R$ as

$$L = L_0/(1 + \beta R), \quad (2)$$

so that Eq. (1) may be rewritten

$$\omega_0[1 - (\sigma_P/\rho\omega_0^2 b^2)]^{1/2} = (\pi^2 G/2\rho)^{1/2}\ (1 + \beta R)/L_0\ . \quad (3)$$

If we can only detect a low-frequency tail $\omega_c$ (the crossover in Figs. 9 and 10) with $\omega_0 = \omega_c\delta$ or, equivalently, $T_0 = T_c\delta$, Eq. (3) becomes

$$T_x \equiv T_c[1 - (\sigma_P/4\pi^2\rho\delta^2 T_c^2 b^2 \times 10^{22})]^{1/2} = (G/2\rho)^{1/2}\ (1 + \beta R)/(2\delta L_0 \times 10^{11}). \quad (4)$$

A plot of $T_x$ vs $R$ is shown in Fig. 15. One could take the broken line as a reasonable fit to badly scattered data; that is, assume that the Peierls potential is effectively zero and that our previous discussion of average loop length and scattering magnitude was appropriate. On the other hand, one could take the data at face value as shown by the solid lines of Fig. 15 meaning that

$$[1 - (\sigma_P/4\pi^2\rho\delta^2 T_c^2 b^2 \times 10^{22})]^{1/2} \approx 0$$

at $R = 0$. Taking the broken and solid lines to represent reasonable limits set by the data gives

$$0 < (\sigma_P/\delta^2) \lesssim 10^6 \text{ dyn/cm}^2, \quad L_0\delta \gtrsim 4 \times 10^{-5} \text{ cm}, \quad (5)$$

assuming $b \simeq 3 \times 10^{-8}$ cm, $\rho \simeq 2.7$ g/cm$^3$, $T_c \simeq 0.04$ K, and $G \simeq 5.4 \times 10^{11}$ dyn/cm$^2$. A value for $\delta$ of roughly 5 can be estimated from a comparison of Fig. 14 and Figs. 9 and 10. For $\delta = 5$,

$$0 < \sigma_P \lesssim 3 \times 10^7 \text{ dyn/cm}^2, \quad L_0 \gtrsim 10^{-5} \text{ cm}. \quad (6)$$

Hence for a freshly strained crystal we need not postulate a set of weak pinning points if a Peierls stress of order $10^7$ dyn/cm$^2$ exists in LiF. Values of $\sigma_P$ for LiF quoted in the literature have a range of $(5-50) \times 10^7$ dyn/cm$^2$ as obtained by the use of data involving macroscopic motion of the sample and a specific model of dislocation behavior.[42–45] Hence the present sparse data suggest a value of the Peierls stress which is somewhat smaller than the earlier deductions. More of the present type of data at low-irradiation doses could establish an accurate value for $\sigma_P$.

It is interesting to note that the saturation observed in Fig. 11 is very similar to the behavior of certain properties of NaCl with $\gamma$ irradiation,[46, 47] the saturation effects even occurring at a similar irradiation level corresponding to a color center density of $10^{15}$–$10^{16}$ cm$^{-3}$. In brief, it may be said that irradiation hardening, the rate of $F$-center production, and the change in the average loop length $L_0$ all follow a similar curve versus irradiation dose. If the efficiency of $F$-center production is roughly the same in LiF as in NaCl, the dislocations in the present work would require an effective radius of $\approx 10^2 b$ if the point defects were distributed at random throughout the crystal. This plus the enhanced coloration observed in the strained region is further evidence that the $F$ centers collect or, rather, are produced at the dislocations during the first stage of irradiation damage. The saturation effects referred to above might then correspond to a maximum number of point defects situated in thermodynamic equilibrium along the dislocations.

In this section the discussion has ranged from a statement of fact to areas of increasing speculation. No attempt has been made to discuss all dislocation models or theories,[1] although most are variations on the models that have been considered above.

## V. CONCLUSIONS

The interaction between thermal phonons and dislocations in LiF has been studied by means of

thermal-conductivity measurements and by observation of the ballistic propagation of thermal phonon pulses. For a crystal deformed by shear the slow transverse phonons are scattered strongly and dynamically by dislocations. With sufficient exposure to $\gamma$ irradiation, resulting in pinning of mobile dislocations, the scattering of all three phonon modes becomes too small to detect below $\approx 1$ K.

The data are consistent with earlier measurements on LiF. These previous data may be understood more readily in terms of the observations made above rather than in terms of previously proposed *ad hoc* scattering processes.

The elastic string model of a mobile dislocation accounts adequately for the present data provided (i) the "fluttering" mechanism investigated by Ninomiya[13] is included and provided (ii) that either the average effective loop length is very short for a freshly deformed crystal (perhaps due to a set of weak pinning centers) or that a Peierls potential, consistent in magnitude with previous estimates, is operative. For sessile dislocations the scattering cross section calculated by Ohashi[5] is much too large, whereas that calculated by Klemens[2] and by Carruthers[3] would be consistent with the present data.

*Note added in proof.* Thermal-conductivity data for deformed LiF crystals at temperatures above 1.5 K have recently been published by T. Suzuki and H. Suzuki, J. Phys. Soc. Japan 32, 164 (1972). Their results are consistent with those of the present paper.

## ACKNOWLEDGMENTS

The interest of A. V. Granato and G. Wire in this work has been very helpful and is greatly appreciated by the authors.

---

† Work supported in part by the Advanced Research Projects Agency under Contract No. HC 15-67-C0221.

‡A portion of this paper is based upon a dissertation submitted by M. E. Malinowski in partial fulfillment of the requirements for the Ph. D. degree at the University of Illinois, Urbana, Ill. 61801.

*Present address: Sandia Laboratories, Livermore, Calif. 94550.

[1]The literature on the concepts and practices mentioned in the present article is voluminous. For a reasonable review and bibliography of the literature prior to 1963, see (a) J. Friedel, *Dislocations* (Addison-Wesley, Reading, Mass., 1964). For more recent commentary, see (b) *Dislocation Dynamics*, edited by A. R. Rosenfield, G. T. Hahn, A. L. Bement, and R. I. Jaffee (McGraw-Hill, New York, 1968); (c) *Fundamental Aspects of Dislocation Theory*, edited by J. A. Simmons, R. De Wit, and R. Bullough (U. S. GPO, Washington, D. C., 1970), Natl. Bur. Std. Spec. Publ. 317.

[2]P. G. Klemens, in *Solid State Physics*, edited by D. Turnbull and F. Seitz (Academic, New York, 1958), Vol. 7, p. 1; plus earlier papers cited therein.

[3]P. Carruthers, Rev. Mod. Phys. 33, 92 (1961).

[4]M. Moss, J. Appl. Phys. 37, 4168 (1966).

[5]K. Ohashi, J. Phys. Soc. Japan 24, 437 (1968).

[6]R. L. Sproull, M. Moss, and H. Weinstock, J. Appl. Phys. 30, 334 (1959).

[7]A. Taylor, H. R. Albers, and R. O. Pohl, J. Appl. Phys. 36, 2270 (1965).

[8]P. Gruner and H. Bross, Phys. Rev. 172, 583 (1968).

[9]M. W. Ackerman and P. G. Klemens, Phys. Rev. B 3, 2375 (1971).

[10]For example see the discussion in J. Phys. Soc. Japan Suppl. II 18, 97 (1963).

[11]A. Granato, Phys. Rev. 111, 740 (1958).

[12]S. Ishioko and H. Suzuki, J. Phys. Soc. Japan Suppl. II 18, 93 (1963).

[13]T. Ninomiya, in Ref. 1(c), p. 315, papers cited therein.

[14]R. O. Schwenker and A. V. Granato, Phys. Rev. Letters 23, 918 (1969); J. Phys. Chem. Solids 31, 1869 (1970).

[15]R. B. Gordon and A. S. Nowick, Acta Met. 4, 514 (1956).

[16]T. Ochs, J. Sci. Instr. 1, 1122 (1968).

[17]J. J. Gilman and W. G. Johnston, in *Solid State Physics*, edited by F. Seitz and D. Turnbull (Academic, New York, 1962), Vol. 13, p. 147; see also F. Fanti, J. Holder, and A. V. Granato, J. Acoust. Soc. Am. 45, 1356 (1969).

[18]The following etching procedure was used: (i) etch in concentrated HF acid for 30–60 sec; (ii) polish with agitation in fresh solution of 0.5–1% $NH_4OH$ in distilled $H_2O$ for 30–60 min; (iii) etch in 50: 50 solution of HF: $CH_3COOH$ plus 0.5–1% HF saturated with $FeCl_3$, for 30–60 sec; (iv) rinse in absolute ethanol then ether after each step. The resulting pits were sharply defined and had the expected orientation.

[19]A. C. Anderson and J. E. Robichaux, Rev. Sci. Instr. 40, 1512 (1969).

[20]A. C. Anderson, R. E. Peterson, and J. E. Robichaux, Rev. Sci. Instr. 41, 528 (1970).

[21]R. J. von Gutfeld, in *Physical Acoustics*, edited by W. P. Mason (Academic, New York, 1968), Vol. 5, p. 233; plus earlier papers cited therein.

[22]B. Taylor, H. J. Maris, and C. Elbaum, Phys. Rev. B 3, 1462 (1971).

[23]S. J. Rogers, Phys. Rev. B 3, 1440 (1971).

[24]J. P. Harrison, Rev. Sci. Instr. 39, 145 (1968).

[25]M. W. Wolfmeyer and J. R. Dillinger, Phys. Letters 34A, 247 (1971).

[26]A. K. McCurdy, H. J. Maris, and C. Elbaum, Phys. Rev. B 2, 4077 (1970).

[27]R. Berman, F. E. Simon, and J. M. Ziman, Proc. Roy. Soc. (London) A220, 171 (1953).

[28]A. F. Cohen, in Oak Ridge National Laboratory Solid State Division Annual Progress Report ORNL-2614 T1D-4500, 19th ed., 1958, p. 39 (unpublished); R. O. Pohl, Phys. Rev. 118, 1499 (1960); the expected $T^{-4}$ dependence of the phonon mean free path was not observed by these authors.

[29]M. Peach and J. S. Koehler, Phys. Rev. 80, 436 (1950). This equation, $d\vec{F} = (\vec{b} \cdot \vec{\sigma}) \times d\vec{l}$, gives the force $d\vec{F}$ on a dislocation line element $d\vec{l}$ resulting from an applied stress $\vec{\sigma}$. Here $\vec{b}$ is the Burgers vector.

[30]P. D. Thacher, Phys. Rev. 156, 975 (1967).
[31]T. Suzuki (private communication); these data also appear in Fig. 8 of Ref. 13.
[32]S. C. Smith, Ph. D. dissertation (University of Illinois, 1971) (unpublished); A. C. Anderson and S. C. Smith (unpublished); see also J. K. Wigmore, Phys. Letters 37A, 293 (1971).
[33]Within this model, the number of kinks would presumably be constant at the temperature and vibrational amplitudes of the present experiment.
[34]T. Holstein, Phys. Rev. 83, 1159 (1951).
[35]J. A. Garber and A. V. Granato, J. Phys. Chem. Solids 31, 1863 (1970); in Ref. 1(c), p. 419.
[36]J. S. Koehler, in *Imperfections in Nearly Perfect Crystals*, edited by W. Shockley, J. H. Holloman, R. Maurer, and F. Seitz (Wiley, New York, 1952), p. 197.
[37]A. V. Granato and K. Lücke, Phys. Acoust. 4A, 225 (1966).
[38]A. V. Granato, in Ref. 1(b), p. 117.
[39]W. S. de Rosset and A. V. Granato, J. Appl. Phys. 41, 4105 (1970).
[40]J. D. Eshelby, Proc. Roy. Soc. (London) A266, 222 (1962).
[41]T. Suzuki and C. Elbaum, J. Appl. Phys. 35, 1539 (1964); R. Truell, C. Elbaum, and R. R. Chick, in *Ultrasonic Methods in Solid State Physics* (Academic, New York, 1969), p. 190. The latter reference also presents a brief introduction to the string and kink models.
[42]A. Taylor, Acta Met. 10, 223 (1962).
[43]A. Ikushima and T. Suzuki, J. Phys. Soc. Japan Suppl. I 18, 163 (1963).
[44]P. Guyat and J. E. Dorn, Can. J. Phys. 45, 983 (1967).
[45]T. Takeuchi, J. Phys. Soc. Japan 17, 659 (1962).
[46]I. S. Lerma and F. Agullo-Lopez, J. Appl. Phys. 41, 4628 (1970).
[47]Ya. M. Soifer, Phys. Status Solidi A 4, 333 (1971).

PHYSICAL REVIEW B VOLUME 5, NUMBER 8 15 APRIL 1972

# Properties of Crystalline Argon, Krypton, and Xenon Based Upon the Born-Huang Method of Homogeneous Deformations. III. The Low-Temperature Limit*

G. E. Jelinek
*Sandia Laboratories, Albuquerque, New Mexico* 87115
(Received 5 November 1971)

The low-temperature limits of the thermal expansivity, specific heat, and Grüneisen parameter of solid argon, krypton, and xenon are calculated from a quasiharmonic two-body central-force model. The form of our interatomic potential and its predicted thermal and elastic properties are in good agreement with interatomic potentials for argon and krypton derived from solid-state properties plus gas viscosities, second-virial coefficients, and molecular-beam scattering data.

## I. INTRODUCTION

In Paper I of this series[1] we developed our model for the thermodynamics of a stressed harmonic lattice, based upon Born and Huang's[2] perturbation expansion of the partition function. Anharmonic effects due to thermal expansion were calculated for strains taken to be homogeneous deformations; the Helmholtz free energy was obtained as a series expansion in the Lagrangian strain parameters. In Paper I the nonarbitrarily adjustable parameters of a central-force potential were determined completely from the zero-pressure experimental sublimation energy, density, and bulk modulus of the solid in a recursive refinement procedure [see Eq. (I 4)]. In Paper II[3] pressure-volume-temperature relationships of our model of argon, krypton, and xenon were compared with the static compression data, which extended to 20 kbar.

Tilford and Swenson[4] using a three-terminal capacitance dilatometer recently measured the thermal expansion coefficients of solid argon, krypton, and xenon at temperatures down to 1 K with a resolution of $10^{-10}$ in the relative length change of the specimen. Prediction of the temperature dependence of the thermal expansion coefficient $\alpha = \beta_T(\partial^2 F/\partial T \partial V)$ is a very severe test of the theory, since $\alpha$ is a mixed second derivative of the Helmholtz free energy. The purpose of this investigation is to calculate and compare with these recent data our predictions, in the low-temperature limit, of the coefficient of thermal expansion, the constant-volume specific heat, and the Grüneisen parameter. We will also compare the Morse and exp-6 potentials of our model with the 13-parameter analytic potential of Bobetic and Barker[5] for argon and of Barker, Bobetic, and Klein[6] for krypton. We will discuss a discrepancy in the low-temperature elastic data of argon which exists between theory and experiment.

## II. POTENTIAL MODELS

The Morse potential is given by

$$\phi(r) = \epsilon\left[-e^{-2\alpha(r-r_0)} + 2e^{-\alpha(r-r_0)}\right]. \quad (1)$$